Applied Catalysis B: Environmental 245 (2019) 656–661

Contents lists available at ScienceDirect

Applied Catalysis B: Environmental

journal homepage: www.elsevier.com/locate/apcatb

Ultra-dispersed molybdenum phosphide and phosphosulfide nanoparticles on hierarchical carbonaceous scaffolds for hydrogen evolution electrocatalysis

Yang Huang[1], Xuening Song[1], Jun Deng, Chenyang Zha, Wenjing Huang, Yunling Wu, Yanguang Li*

Institute of Functional Nano and Soft Materials (FUNSOM), Jiangsu Key Laboratory for Carbon-Based Functional Materials and Devices, Soochow University, Suzhou, 215123, China

ARTICLE INFO

Keywords:
Molybdenum phosphide
Ultra-dispersed nanoparticles
Three-dimensional hierarchical structure
Electrocatalytic hydrogen evolution
sulfur doping

ABSTRACT

Transition metal phosphides are arguably the most promising non-precious metal-based materials for hydrogen evolution reaction (HER). Unfortunately, their high preparation temperature usually results in particle sintering. It is challenging to achieve the ultra-dispersion of transition metal phosphide nanoparticles on conductive supports so as to enlarge their surface areas and reinforce their physical stability. In this study, we prepare fine MoP nanoparticles uniformly dispersed on hierarchical carbonaceous scaffolds by using strongly interacting Mo, P and C precursors. The resultant hybrid product possesses a three-dimensional open structure that allows a large fraction of MoP nanoparticles electrochemically accessible and suppresses their possible agglomeration during extended electrocatalysis. Electrochemical measurements show that the product has an impressive HER activity, only requiring an overpotential of 120 and 170 mV to achieve 10 mA/cm^2 in 0.5 M H_2SO_4 and 1M KOH, respectively, as well as great cycling stability. Its performance can be further promoted via the controlled sulfur doping at surface to form molybdenum phosphosulfide, which reduces the overpotential at j = 10 mA/cm^2 to 92 mV and 158 mV for acidic and alkaline HER.

1. Introduction

Water electrolysis using renewable energy sources such as solar and wind represents an attractive route for hydrogen production [1,2]. It involves hydrogen evolution reaction (HER) at the cathode and oxygen evolution reaction (OER) at the anode, and typically requires the assistance of electrocatalysts so as to reduce the reaction overpotentials and accelerate the reaction rates. Current interest for developing HER electrocatalysts has gradually shifted away from noble metals (such as Pt and Pd) to non-precious metal-based alternatives with comparable activity and at much lower cost [2–7]. Transition metal phosphides (TMPs) are a large group of materials, which are traditionally well known for their applications in hydrogenation catalysis [8]. It was not until 2013 that their great potential in HER started to attract widespread interest [9]. Currently TMPs are the arguably best non-precious metal-based HER electrocatalysts [10–18]. It is believed that phosphorus atoms doped in the metal lattices are crucial for the high activity by affording TMPs with noble metal like properties and acting as the "hydrogen deliverer" during HER [19]. As one of the most studied TMPs, molybdenum phosphide exhibits impressive HER activity in both acidic and alkaline media [19–23]. Unfortunately, its preparation generally demands high-temperature phosphidation, which often leads to extensive particle sintering [10,19,24]. Some attempts have been made to mitigate this issue. For example, Sun and coworkers introduced citric acid as the chelating agent and obtained a closely interconnected network of MoP nanoparticles with enlarged surface areas and improved HER performance [23]. However, even with this strategy, the particle size was still relatively large (~50 nm).

We propose that by properly selecting the starting molybdenum, phosphorus and carbon precursors with strong mutual interactions, one may effectively suppress the sintering of MoP nanoparticles during high-temperature annealing and achieve their ultra-dispersion on carbonaceous supports. These supports preferably have great surface areas and abundant porosity in order to render MoP nanoparticles electrochemically accessible, as well as mechanical robustness in order to preserve the overall structural integrity during extended

* Corresponding author.
E-mail address: yanguang@suda.edu.cn (Y. Li).
[1] These two authors contribute equally to this work.

https://doi.org/10.1016/j.apcatb.2019.01.034
Received 24 August 2018; Received in revised form 8 January 2019; Accepted 13 January 2019
Available online 14 January 2019
0926-3373/

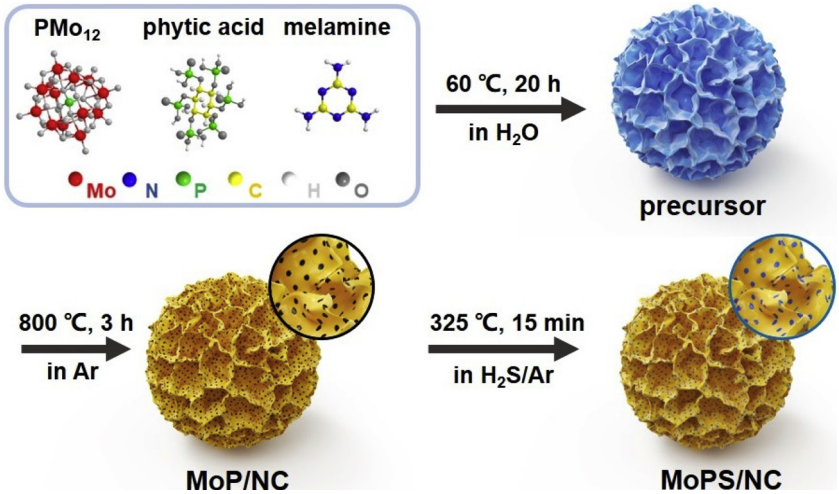

Fig. 1. Schematic synthetic process of MoP/NC and MoPS/NC.

electrocatalysis. Guided by this design principle, we here describe a straightforward two-step method to prepare non-sintered MoP nanoparticles using strongly interacting precursors. The final product features fine MoP nanoparticles uniformly dispersed on three-dimensional (3D) hierarchical carbonaceous scaffolds. It exhibits excellent electrocatalytic activity and stability for HER in both acidic and alkaline solution. The performance can be further promoted via the controlled sulfur doping at surface to form phosphosulfide (MoPS).

2. Experimental

2.1. Materials

All chemicals were of reagent grade and used without further purifications. 12-Molybdophosphoric acid hydrate ($H_3PO_4{\cdot}12MoO_3{\cdot}xH_2O$, shorted as PMo_{12}) was purchased from Alfa Aesar. Phytic acid solution ($C_6H_{18}O_{24}P_6$, 70% in H_2O) was purchased from Aladdin. Melamine ($C_3H_6N_6$), ethanol, sulfuric acid (H_2SO_4), and potassium hydroxide (KOH) were purchased from Sinopharm Chemical Reagent Co., China. All solutions were prepared using deionized water.

2.2. Synthesis of MoP/NC and MoPS/NC

In a typical synthesis for MoP/NC, 0.756 g of melamine was first suspended in 50 mL H_2O. It was sequentially added with 4.243 g of phytic acid dispersed in 20 mL H_2O and 0.456 g PMo_{12} dispersed in 30 mL H_2O drop by drop. The resultant suspension was then heated at 60 ℃ and magnetically stirred for 20 h. Solid product was collected by centrifugation, washed three times with deionized water, and lyophilized. Subsequently, the solid powder was annealed in Ar at 800 ℃ for 3 h with a temperature ramping rate of 10 ℃·min^{-1} to form MoP/NC. In order to prepare MoPS/NC, above MoP/NC was additionally treated with 10% H_2S in Ar at 325 ℃ for 15 min.

2.3. Structural characterizations

X-ray diffraction (XRD) patterns were obtained on a PANalytical X-ray diffractometer using Cu Kα radiation (40 kV, 40 mA). Scanning electron microscopy (SEM) images were taken from a Zeiss scanning electron microscope. Transmission electron microscopy (TEM) images and scanning transmission electron microscopy (STEM) analyses were performed on an FEI Tecnai F20 transmission electron microscope operating at an acceleration voltage of 200 kV. X-ray photoelectron spectroscopy (XPS) spectra were obtained on an ESCALAB 250 XI XPS spectrometer. Inductive coupled plasma (ICP) measurements were conducted on Varian Vista MPX. Samples were digested in concentrated HNO_3 and diluted to desired concentrations.

2.4. Electrochemical measurements

To prepare the working electrode, 1 mg of catalyst powder, 0.5 mg of Ketjenblack carbon black and 8 μL of 5 wt% Nafion solution were first dispersed in 125 μL water and 125 μL ethanol, and vigorously sonicated for 40 min to form a homogeneous ink. 10 μL of the ink was then loaded onto a glassy carbon electrode (with a diameter of 3 mm) to reach an areal density of ~0.56 mg/cm^2. HER measurements were carried out at a standard three-electrode configuration using a saturated calomel electrode (SCE) and a graphite rod as the reference and counter electrodes, respectively. The electrolyte was 0.5 M H_2SO_4 or 1 M KOH. All the potential readings were corrected for the ohmic loss and reported with respect to reversible hydrogen electrode (RHE). Polarization curves were recorded at the scan rate of 10 mV/s.

3. Results and discussion

3.1. Preparation and structural characterizations of MoP/NC

Fig. 1 schematically summarizes the synthetic procedure for MoP and MoPS nanoparticles ultra-dispersed on 3D N-doped carbonaceous scaffolds (MoP/NC or MoPS/NC). Phosphomolybdic acid ($H_3PMo_{12}O_{40}$ or PMo_{12}), phytic acid ($C_6H_{18}O_{24}P_6$) and melamine ($C_3H_6N_6$) are used as the molybdenum, phosphorus and carbon precursors, respectively. This combination is chosen based on the following consideration. Phytic acid is a naturally occurring biomolecule containing six phosphate groups. Such a unique structure allows it to readily chelate or interact with the metal precursor and melamine at the same time, serving as a crosslinker while providing the necessary phosphorus species [25–27]. The choice of PMo_{12} is prompted by some previous studies for its capability to afford small and uniform Mo-based (Mo_2C and Mo_2N) nanostructures [28,29]. Melamine is preferred for its characteristic self-polymerization at elevated temperatures, which may further react and transform to N-doped carbonaceous materials. In our experiment, the three precursors were first dispersed in aqueous solution and mildly heated to react. Resultant solid precipitate was collected and characterized by XRD and SEM as shown in Figure S1. This precipitate was then annealed at 800 ℃ for 3 h.

We interrogated the composition and structure of MoP/NC using different spectroscopic and microscopic techniques. Its powdered XRD pattern supports the successful formation of hexagonal MoP phase with no discernible impurity (Fig. 2a). The particle size is estimated to be

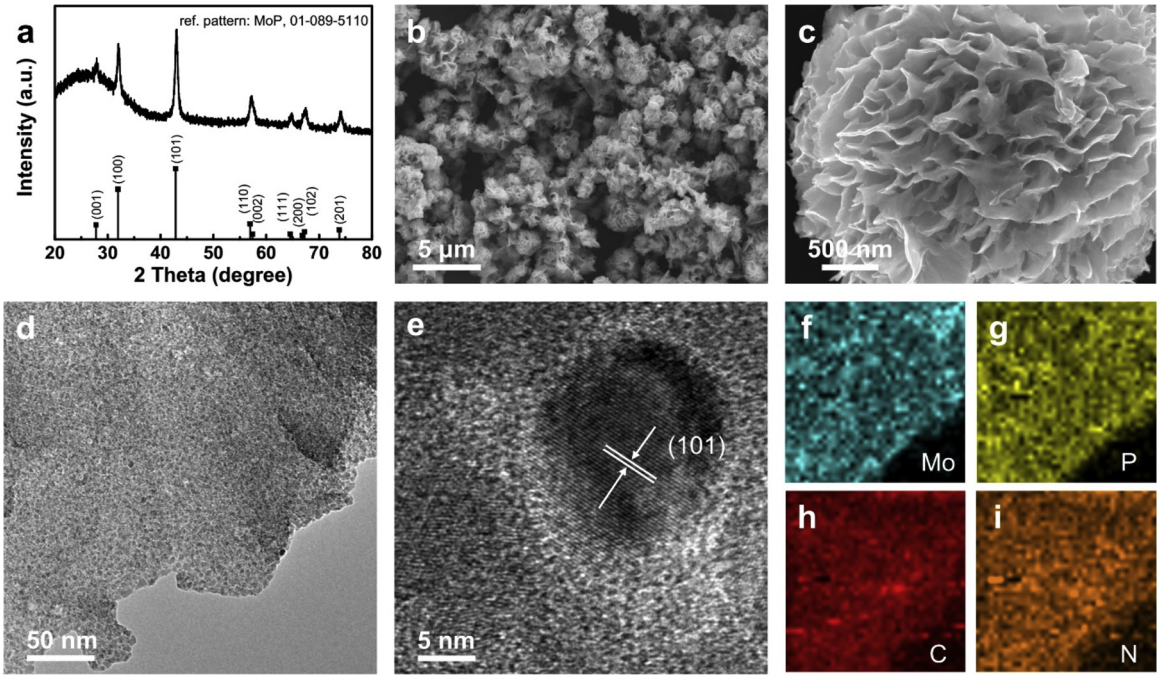

Fig. 2. Structural characterizations of MoP/NC. (a) XRD pattern, (b, c) SEM images, (d, e) TEM images, and (f–i) EDS elemental mapping of Mo, P, C and N species.

~15 nm based on the strongest (101) peak via the Scherrer equation. SEM image shows that the final product consists of flower-like microstructures about 1.5–3 μm in diameter (Fig. 2b). Each microflower is assembled from many thin nanoflakes that are hierarchically arranged with little overlapping (Fig. 2c). The open space between neighboring nanoflakes ensures that even the core region is accessible from the outside. Under TEM, numerous dark contrasted nanoparticles about 5~15 nm in size are observed to be evenly dispersed over individual nanoflakes (Fig. 2d**)**. Close examination reveals that these nanoparticles are crystalline and display obvious lattice fringes such as those from the (101) plane (Fig. 2e). Energy dispersive spectroscopy (EDS) elemental mapping of Mo, P, C and N under STEM evidences that all four constituent elements have high spatial correlation, which clearly reflects the uniform dispersion of MoP nanoparticles on the N-doped carbonaceous support in MoP/NC (Fig. 2f–i). Moreover, XPS characterization of MoP/NC was carried out and results are summarized in **Figure S2**. The surface Mo/P molar ratio is estimated to be ~1.3. Its Mo 3d spectrum is deconvoluted to three sets of doublets. The one at 228.3/231.4 eV is consistent with Mo in MoP, while the other two sets at 229.0/231.4 eV and 232.5/235.9 eV are attributable to its surface oxides [19,30,31]. Similarly, the P 2p spectrum features two sets of doublets assignable to P in MoP ($2p_{3/2}$ at 129.4 eV) and surface phosphate ($2p_{3/2}$ at 134.2 eV) [32]. The surface oxidation is common to all TMPs when they are exposed to air. N 1 s spectrum evidences that pyridinic N is the predominant N species as inherited from melamine. ICP analysis shows that the final product contains ~48 wt% Mo, which corresponds to ~64 wt% MoP in MoP/NC. Raman spectrum of MoP/NC in **Figure S3** indicates that the carbonaceous support is partially graphitic.

We believe that the formation of ultra-dispersed MoP nanoparticles on hierarchical N-doped carbonaceous scaffolds is a direct consequence of the strong interplay among PMo_{12}, phytic acid and melamine. Phytic acid plays an important role by crosslinking PMo_{12} and melamine together, ensuring their homogeneous mixing at the atomic level. Replacing phytic acid with an equivalent amount of phosphoric acid under otherwise identical conditions gives rise to elongated MoP_3/Mo_8P_5 particles of submicron size (**Figure S4a-c)**. PMo_{12} is also found decisive to the formation of fine MoP nanoparticles. Replacing PMo_{12} with an equivalent amount of $(NH_4)_6Mo_7O_{24}$ under otherwise identical conditions results in an interconnected MoP_3/Mo network (**Figure S4d-f**). Moreover, self-polymerized melamine serves as the template that ultimately transforms to the 3D N-doped carbonaceous scaffolds. The final product MoP/NC possesses large surface areas, hierarchical order at different levels, and sufficient mechanical robustness. These structural advantages render it an ideal material for electrocatalysis.

3.2. HER performance of MoP/NC

The HER performance of MoP/NC was assessed in both acidic and alkaline solution using the standard three-electrode configuration. The catalyst powder was blended with carbon black and Nafion binder, dispersed in H_2O/ethanol to form a homogeneous catalyst ink, and then dropcast onto glassy carbon electrodes. For the purpose of comparison, commercial 20 wt % Pt/C was also introduced as the benchmark and tested side by side. Fig. 3**a** depicts the HER polarization curve of MoP/NC and Pt/C in 0.5 M H_2SO_4. Pt/C is well known for its excellent HER activity in acids with negligible overpotential, which is again confirmed from our measurement. As for MoP/NC, a positive onset potential (defined as the potential to reach 0.5 mA/cm^2) of -0.055 V (versus RHE, the same hereafter) is observed. Once taking off, the HER current density continuously rises, and reaches 10 and 20 mA/cm^2 at -0.12 V and -0.14 V, respectively. Tafel analysis gives rise to a slope of ~52 mV/decade (Fig. 3**a inset**). Compared to HER in acids, HER in alkaline solution is considerably more challenging due to its slower water dissociation step (about two to three orders of magnitude slower than the discharge of protons in acids) [33,34]. It is therefore remarkable that our MoP/NC also exhibits an impressive HER activity in 1 M KOH, and is capable of delivering a cathodic current density of 10 and 20 mA/cm^2 at -0.17 and -0.20 V, respectively (Fig. 3b). Corresponding Tafel slope is estimated to be ~50 mV/decade (Fig. 3b inset). Even though still inferior to the best Pt/C benchmark, we find that the HER activity of our MoP/NC compares favorably to most previous MoP-based materials as well as Mo-based sulfides, nitrides and carbides as summarized in **Table S1** of the Supporting Information [19,23,24,30,35–39].

We attribute the great HER performance of MoP/NC to its unique structure. Individual MoP nanoparticles have small sizes and are uniformly dispersed over the 3D hierarchical scaffolds. This renders a great fraction of catalytically active sites accessible from surface. The ultra-

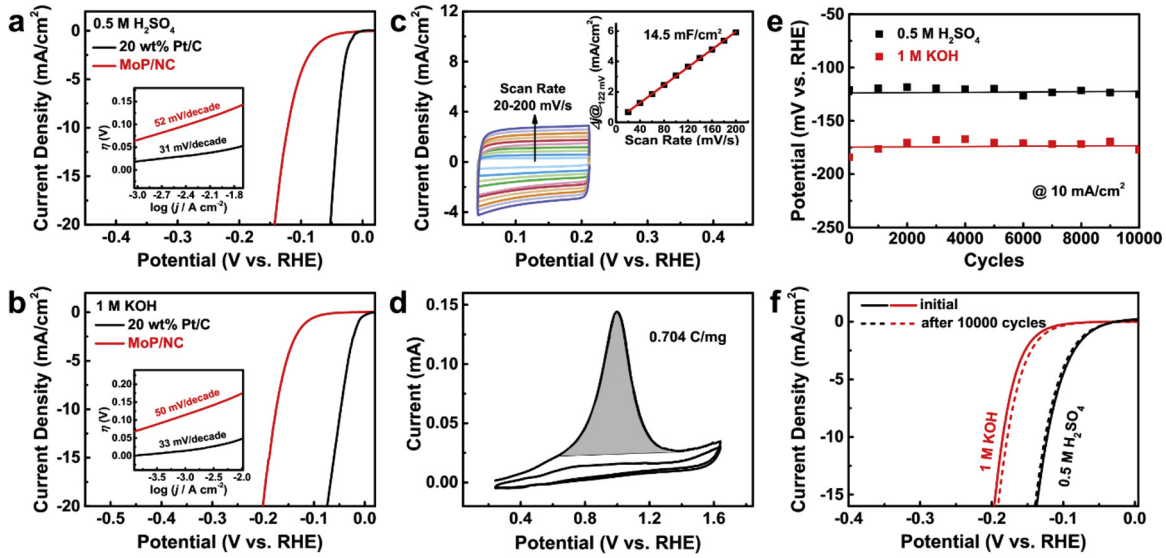

Fig. 3. Electrochemical measurements of MoP/NC. (a,b) Polarization curves of MoP/NC and 20 wt% Pt/C in (a) 0.5 M H_2SO_4 and (b) 1 M KOH, insets show the corresponding Tafel plots; (c) CV curves of MoP/NC within a non-Faradaic potential region under various scan rates in 0.5 M H_2SO_4, inset illustrates the dependence of the capacitive current density at 0.122 V on the scan rate; (d) CV curves of MoP/NC at anodic potentials showing the oxidation of MoP/NC, the fraction of exposed MoP was calculated based on the integrated area of the anodic wave; (e) change of the working potential at 10 mA/cm^2 with the number of CV cycles; (f) polarization curves of MoP/NC before and after 10,000 CV cycles.

dispersion of MoP on the conductive scaffolds also facilitates the rapid charge transfer to and from the catalytically active sites. In order to estimate the electrochemical surface area (ECSA) of MoP/NC, two different methods were undertaken as detailed below. First, ECSA was calculated based on its double-layer capacitance. To achieve this, cyclic voltammetry (CV) curves at different scan rates were collected in a non-Faradaic potential region of 0.06-0.21 V (Fig. 3c). The difference between the cathodic and anodic current density at 0.122 V was then plotted against the scan rate. Fitting the data discloses a good linear correlation with a slope of ~25.9 F/g. By assuming a standard value of 40 μF/cm^2 (common for many oxide surfaces), [40–42] we estimate the ECSA of MoP/NC to be ~64 m^2/g — a considerably high value given the heavy density of MoP. Worth noting is that the thus-derived ECSA includes the contribution from the support material, and may not reflect the true surface area of the electrocatalytically active component. To this end, MoP/NC was additionally subjected to irreversible electrochemical oxidation by applying an anodic sweep until the evolution of oxygen (Fig. 3d). A pronounced anodic wave is observed between 0.6 V and 1.4 V. From the charge integrated over this anodic wave and by assuming an 11-electron transfer process for its complete oxidation, we estimate ~13.6% of MoP is electrochemically accessible on surface (see calculation details in Supporting Method 1).

Next, we investigated the long-term cycling stability of MoP/NC. The working electrode was continuously run for a total of 10,000 CV cycles at 100 mV/s between -0.14 − 0.04 V and -0.18 − 0.07 V in acidic and alkaline solution, respectively. Its HER activity was monitored by periodically collecting the polarization curve every 1000 cycles, extracting the working potential at j = 10 mA/cm^2, and then plotting the potential against the cycle number. Despite some fluctuation, it is observed that the working potential roughly maintains at -0.12 V in 0.5 M H_2SO_4 and at -0.17 V in 1 M KOH (Fig. 3e). Comparison of the polarization curves before and after 10,000 cycles indicates negligible activity decay (Fig. 3f). Moreover, SEM and TEM images of MoP/NC after the long-term cycling test reveals that its structural integrity and hierarchical order are well maintained (**Figure S5**). There is no sign of MoP nanoparticle agglomeration. In addition, MoP/NC was soaked in 0.5 M H_2SO_4 or 1 M KOH at room temperature for 5 h. No leaching of any Mo out of the catalyst was identified by ICP analysis within the instrument's detection limit, indicating its good chemical stability.

3.3. Preparation and HER performance of MoPS/NC

At last, in order to further promote the HER performance, we carried out the controlled S doping of MoP/NC at surface. It was suggested that the S doping could play a positive role by generating a mixed-anion phase of phosphosulfide which was more active for HER [43,44]. Theorical calculations showed that the synergistic effect between S and P could modify the free energy of H adsorption, moving the phosphosulfide in the volcano plot closer to the peak than pristine MoP [43–45]. However, there have been few demonstrations about the successful S doping of MoP [22,43,44]. To achieve so, as-prepared MoP/NC in our experiment was reacted with diluted H_2S gas at 320 °C for 15 min. The sulfidation temperature and time affect the S doping level and are thereby critical to the electrochemical performance of MoPS/NC (Figure S6). Controlled S doping does not cause a noticeable structure change. XRD shows that the crystalline MoP phase is retained (**Figure S7**). SEM and TEM characterizations reveal that MoPS/NC has similar 3D hierarchical microstructures assembled from numerous nanoflakes (Fig. 4a), and that fine MoPS nanoparticles are uniformly dispersed on individual nanoflakes (Fig. 4b). The successful S doping in MoPS/NC becomes evident from EDS elemental mapping (Fig. 4c–e). Its signal distributes over the entire nanoflake, suggesting that the doping is overall homogeneous. In addition, XPS of MoPS/NC exhibits similar Mo 3d, P 2p, N 1 s and C 1 s spectral features as MoP/NC (**Figure S8**). Careful analysis of its S 2p spectrum uncovers the contribution from the direct Mo-S bonding [43]. The surface S/P atomic ratio is estimated to be 0.33 by XPS. ICP analysis suggests that the Mo content in MoPS/NC is ~53 wt%. Furthermore, the HER performance of MoPS/NC was likewise evaluated and compared to that of MoP/NC. The controlled S doping is observed to substantially improve the electrocatalytic activity. The onset potential of MoPS/NC is positively displaced to -0.023 V in 0.5 M H_2SO_4 and -0.077 V in 1 M KOH (Fig. 4f and g). It only takes an overpotential of 92 mV and 158 mV to reach j = 10 mA/cm^2 in the acidic and alkaline solution, respectively. Their Tafel plots were shown in **Figure S9**. Such a high activity places our MoPS/NC on top of most other non-precious metal-based HER electrocatalysts (**Table S1**). The excellent HER performance of MoPS/NC observed here is not only attributed to its small particle size and large electrochemical surface area, but also the proper surface doping with S, which may modify the

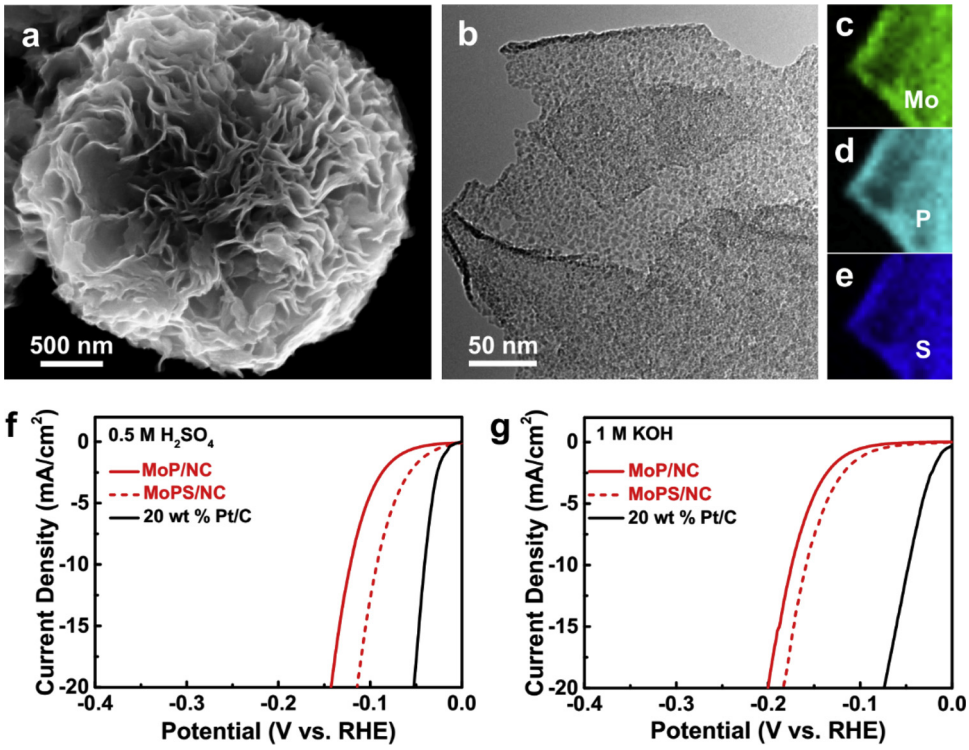

Fig. 4. Structural characterizations and electrochemical measurements of MoPS/NC. (a) SEM image, (b) TEM image, and (c–d) EDS mapping of MoPS/NC; (f,g) polarization curve of MoPS/NC in comparison with those of MoP/NC and 20 wt% Pt/C in (f) 0.5 M H_2SO_4 and (g) 1 M KOH.

surface electronic state and hence hydrogen adsorption property. Satisfactory cycling stability is also measured (**Figure S10**).

4. Conclusions

In summary, we developed a straightforward method to prepare MoP/NC and MoPS/NC by using strongly interacting PMo_{12}, phytic acid, and melamine as the Mo, P and C precursors. The final products featured ultrafine MoP and MoPS nanoparticles finely dispersed on 3D hierarchical carbonaceous scaffolds. They possessed large surface areas, hierarchical order at different levels, and sufficient mechanical robustness. As a result, the products exhibited excellent electrocatalytic activity and stability for HER in both acidic and alkaline solution. The best catalyst after proper S doping at surface was capable of delivering a cathodic current density of 10 mA/cm^2 at an overpotential of 92 mV and 158 mV in 0.5 M H_2SO_4 and 1 M KOH, respectively. No obvious activity loss was noted even after 10,000 CV cycles. Our study here demonstrates the great potential of MoP/NC and MoPS/NC in HER electrocatalysis.

Acknowledgements

We acknowledge supports from the Priority Academic Program Development of Jiangsu Higher Education Institutions and Collaborative Innovation Center of Suzhou Nano Science and Technology.

Appendix A. Supplementary data

Supplementary material related to this article can be found, in the online version, at doi:https://doi.org/10.1016/j.apcatb.2019.01.034.

References

[1] Z.W. Seh, J. Kibsgaard, C.F. Dickens, I. Chorkendorff, J.K. Norskov, T.F. Jaramillo, Combining theory and experiment in electrocatalysis: insights into materials design, Science 355 (2017) eaad4998.
[2] I. Roger, M.A. Shipman, M.D. Symes, Earth-abundant catalysts for electrochemical and photoelectrochemical water splitting, Int. Rev. Chem. Eng. 1 (2017) 3.
[3] Y.P. Zhu, C. Guo, Y. Zheng, S.Z. Qiao, Surface and interface engineering of noble-metal-free electrocatalysts for efficient energy conversion processes, Acc. Chem. Res. 50 (2017) 915–923.
[4] J. Wang, F. Xu, H.Y. Jin, Y.Q. Chen, Y. Wang, Non-noble metal-based carbon composites in hydrogen evolution reaction: fundamentals to applications, Adv. Mater. 29 (2017) 1605838.
[5] M. Zeng, Y. Li, Recent advances in heterogeneous electrocatalysts for the hydrogen evolution reaction, J. Mater. Chem. A 3 (2015) 14942–14962.
[6] S.Y. Jing, L.S. Zhang, L. Luo, J.J. Lu, S.B. Yin, P.K. Shen, P. Tsiakaras, N-doped porous molybdenum carbide nanobelts as efficient catalysts for hydrogen evolution reaction, Appl. Catal. B-Environ. 224 (2018) 533–540.
[7] Z.Z. Wu, B.Z. Fang, A. Bonakdarpour, A.K. Sun, D.P. Wilkinson, D.Z. Wang, WS2 nanosheets as a highly efficient electrocatalyst for hydrogen evolution reaction, Appl. Catal. B-Environ. 125 (2012) 59–66.
[8] S.T. Oyama, T. Gott, H.Y. Zhao, Y.K. Lee, Transition metal phosphide hydroprocessing catalysts: a review, Catal. Today 143 (2009) 94–107.
[9] E.J. Popczun, J.R. McKone, C.G. Read, A.J. Biacchi, A.M. Wiltrout, N.S. Lewis, R.E. Schaak, Nanostructured nickel phosphide as an electrocatalyst for the hydrogen evolution reaction, J. Am. Chem. Soc. 135 (2013) 9267–9270.
[10] P. Xiao, W. Chen, X. Wang, A review of phosphide-based materials for electrocatalytic hydrogen evolution, Adv. Energy Mater. 5 (2015) 1500985.
[11] Y. Shi, B. Zhang, Recent advances in transition metal phosphide nanomaterials: synthesis and applications in hydrogen evolution reaction, Chem. Soc. Rev. 45 (2016) 1529–1541.
[12] Y. Wang, B. Kong, D. Zhao, H. Wang, C. Selomulya, Strategies for developing transition metal phosphides as heterogeneous electrocatalysts for water splitting, Nano Today 15 (2017) 26–55.
[13] J.H. Wang, W. Cui, Q. Liu, Z.C. Xing, A.M. Asiri, X.P. Sun, Recent progress in cobalt-based heterogeneous catalysts for electrochemical water splitting, Adv. Mater. 28 (2016) 215–230.
[14] J.F. Chang, Q. Lv, G.Q. Li, J.J. Ge, C.P. Liu, W. Xing, Core-shell structured Ni12P5/Ni-3(PO4)(2) hollow spheres as difunctional and efficient electrocatalysts for overall water electrolysis, Appl. Catal. B-Environ. 204 (2017) 486–496.
[15] S.S. Yi, J.M. Yan, B.R. Wulan, S.J. Li, K.H. Liu, Q. Jiang, Noble-metal-free cobalt phosphide modified carbon nitride: an efficient photocatalyst for hydrogen generation, Appl. Catal. B-Environ. 200 (2017) 477–483.
[16] Y. Song, N.J. Li, D.Y. Chen, Q.F. Xu, H. Li, J.H. He, J.M. Lu, 3D ordered MoP inverse opals deposited with CdS quantum dots for enhanced visible light photocatalytic activity, Appl. Catal. B-Environ. 238 (2018) 255–262.
[17] R. Boppella, W.S. Yang, J. Tan, H.C. Kwon, J. Park, J. Moon, Black phosphorus supported Ni_2P Co-catalyst on graphitic carbon nitride enabling simultaneous boosting charge separation and surface reaction, Appl. Catal. B-Environ. 242 (2019)

422–430.
[18] H.W. Man, C.S. Tsang, M.M.J. Li, J.Y. Mo, B.L. Huang, L.Y.S. Lee, Y.C. Leung, K.Y. Wong, S.C.E. Tsang, Transition metal-doped nickel phosphide nanoparticles as electro- and photocatalysts for hydrogen generation reactions, Appl. Catal. B-Environ. 242 (2019) 186–193.
[19] P. Xiao, M.A. Sk, L. Thia, X. Ge, R.J. Lim, J.-Y. Wang, K.H. Lim, X. Wang, Molybdenum phosphide as an efficient electrocatalyst for the hydrogen evolution reaction, Energy Environ. Sci. 7 (2014) 2624–2629.
[20] J.M. McEnaney, J.C. Crompton, J.F. Callejas, E.J. Popczun, A.J. Biacchi, N.S. Lewis, R.E. Schaak, Amorphous molybdenum phosphide nanoparticles for electrocatalytic hydrogen evolution, Chem. Mater. 26 (2014) 4826–4831.
[21] Z. Pu, S. Wei, Z. Chen, S. Mu, Flexible molybdenum phosphide nanosheet array electrodes for hydrogen evolution reaction in a wide pH range, Appl. Catal. B-Environ. 196 (2016) 193–198.
[22] M.A.R. Anjum, J.S. Lee, Sulfur and nitrogen dual-doped molybdenum phosphide nanocrystallites as an active and stable hydrogen evolution reaction electrocatalyst in acidic and alkaline media, ACS Catal. 7 (2017) 3030–3038.
[23] Z. Xing, Q. Liu, A.M. Asiri, X. Sun, Closely interconnected network of molybdenum phosphide nanoparticles: a highly efficient electrocatalyst for generating hydrogen from water, Adv. Mater. 26 (2014) 5702–5707.
[24] J. Jia, W. Zhou, G. Li, L. Yang, Z. Wei, L. Cao, Y. Wu, K. Zhou, S. Chen, Regulated synthesis of Mo sheets and their derivative MoX sheets (X: P, S, or C) as efficient electrocatalysts for hydrogen evolution reactions, ACS Appl. Mater. Inter. 9 (2017) 8041–8046.
[25] K.P. Singh, E.J. Bae, J.-S. Yu, Fe–P: a new class of electroactive catalyst for oxygen reduction reaction, J. Am. Chem. Soc. 137 (2015) 3165–3168.
[26] G. Zhang, G. Wang, Y. Liu, H. Liu, J. Qu, J. Li, Highly active and stable catalysts of phytic acid-derivative transition metal phosphides for full water splitting, J. Am. Chem. Soc. 138 (2016) 14686–14693.
[27] J. Zhang, L. Qu, G. Shi, J. Liu, J. Chen, L. Dai, N,P-Co doped carbon networks as efficient metal-free bifunctional catalysts for oxygen reduction and hydrogen evolution reactions, Angew. Chem. Int. Ed. 55 (2016) 2230–2234.
[28] J.S. Li, Y. Wang, C.H. Liu, S.L. Li, Y.G. Wang, L.Z. Dong, Z.H. Dai, Y.F. Li, Y.Q. Lan, Coupled molybdenum carbide and reduced graphene oxide electrocatalysts for efficient hydrogen evolution, Nat. Commun. 7 (2016) 11204.
[29] H. Yan, Y. Xie, Y. Jiao, A. Wu, C. Tian, X. Zhang, L. Wang, H. Fu, Holey reduced graphene oxide coupled with an Mo_2N–Mo_2C heterojunction for efficient hydrogen evolution, Adv. Mater. 30 (2018) 1704156.
[30] J. Yang, F. Zhang, X. Wang, D. He, G. Wu, Q. Yang, X. Hong, Y. Wu, Y. Li, Porous molybdenum phosphide nano-octahedrons derived from confined phosphorization in UIO-66 for efficient hydrogen evolution, Angew. Chem. Int. Ed. 55 (2016) 12854–12858.
[31] Z. Wu, J. Wang, J. Zhu, J. Guo, W. Xiao, C. Xuan, W. Lei, D. Wang, Highly efficient and stable MoP-RGO nanoparticles as electrocatalysts for hydrogen evolution, Electrochim. Acta 232 (2017) 254–261.
[32] S. Gao, Y. Liu, G.-D. Li, Y. Guo, Y. Zou, X. Zou, General urea-assisted synthesis of carbon-coated metal phosphide nanoparticles for efficient hydrogen evolution electrocatalysis, Electrochim. Acta 199 (2016) 99–107.
[33] N. Danilovic, R. Subbaraman, D. Strmcnik, K.C. Chang, A.P. Paulikas, V.R. Stamenkovic, N.M. Markovic, Enhancing the alkaline hydrogen evolution reaction activity through the bifunctionality of $Ni(OH)_2$/metal catalysts, Angew. Chem. Int. Ed. 51 (2012) 12495–12498.
[34] Y. Zheng, Y. Jiao, A. Vasileff, S.Z. Qiao, The hydrogen evolution reaction in alkaline solution: from theory, single crystal models, to practical electrocatalysts, Angew. Chem. Int. Ed. 57 (2017) 2–14.
[35] W. Cui, Q. Liu, Z. Xing, A.M. Asiri, K.A. Alamry, X. Sun, MoP nanosheets supported on biomass-derived carbon flake: one-step facile preparation and application as a novel high-active electrocatalyst toward hydrogen evolution reaction, Appl. Catal. B-Environ. 164 (2015) 144–150.
[36] Z. Wu, J. Wang, R. Liu, K. Xia, C. Xuan, J. Guo, W. Lei, D. Wang, Facile preparation of carbon sphere supported molybdenum compounds (P, C and S) as hydrogen evolution electrocatalysts in acid and alkaline electrolytes, Nano Energy 32 (2017) 511–519.
[37] Y. Li, H. Wang, L. Xie, Y. Liang, G. Hong, H. Dai, MoS_2 nanoparticles grown on graphene: an advanced catalyst for the hydrogen evolution reaction, J. Am. Chem. Soc. 133 (2011) 7296–7299.
[38] L.F. Pan, Y.H. Li, S. Yang, P.F. Liu, M.Q. Yu, H.G. Yang, Molybdenum carbide stabilized on graphene with high electrocatalytic activity for hydrogen evolution reaction, Chem. Comm. 50 (2014) 13135–13137.
[39] W.-F. Chen, S. Iyer, S. Iyer, K. Sasaki, C.-H. Wang, Y. Zhu, J.T. Muckerman, E. Fujita, Biomass-derived electrocatalytic composites for hydrogen evolution, Energy Environ. Sci. 6 (2013) 1818–1826.
[40] C.C. McCrory, S. Jung, J.C. Peters, T.F. Jaramillo, Benchmarking heterogeneous electrocatalysts for the oxygen evolution reaction, J. Am. Chem. Soc. 135 (2013) 16977–16987.
[41] S. Levine, A.L. Smith, Theory of the differential capacity of the Oxide/Aqueous electrolyte interface, Discuss. Faraday Soc. 52 (1971) 290–301.
[42] Y. Li, P. Hasin, Y. Wu, $Ni_xCo_{3-x}O_4$ nanowire arrays for electrocatalytic oxygen evolution, Adv. Mater. 22 (2010) 1926–1929.
[43] J. Kibsgaard, T.F. Jaramillo, Molybdenum phosphosulfide: an active, acid-stable, earth-abundant catalyst for the hydrogen evolution reaction, Angew. Chem. Int. Ed. 53 (2014) 14433–14437.
[44] R. Ye, P. del Angel-Vicente, Y. Liu, M.J. Arellano-Jimenez, Z. Peng, T. Wang, Y. Li, B.I. Yakobson, S.H. Wei, M.J. Yacaman, J.M. Tour, High-performance hydrogen evolution from $MoS_{2(1-x)}$ $P_{(x)}$ solid solution, Adv. Mater. 28 (2016) 1427–1432.
[45] J. Kibsgaard, C. Tsai, K. Chan, J.D. Benck, J.K. Nørskov, F. Abild-Pedersen, T.F. Jaramillo, Designing an improved transition metal phosphide catalyst for hydrogen evolution using experimental and theoretical trends, Energy Environ. Sci. 8 (2015) 3022–3029.